PROCEEDINGS, 41st Workshop on Geothermal Reservoir Engineering
Stanford University, Stanford, California, February 22-24, 2016
SGP-TR-209

Surface Reflection Seismic and Vertical Seismic Profile at Brady's Hot Springs, NV, USA

John H. Queen[1], Thomas M. Daley[2], Ernest L. Majer[2], Kurt T. Nihei[2], Drew L. Siler[2] and James E. Faulds[3]

[1]Hi-Q Geophysical Inc. 106 Fairview Avenue, Ponca City, OK 74601, USA
[2]Earth Sciences Division, Lawrence Berkeley National Laboratory, 1 Cyclotron Road, Berkeley, CA 94720, USA
[3]Nevada Bureau of Mines and Geology, University of Nevada, Reno, NV 89557, USA

john.h.queen@gmail.com

Keywords: seismic, vertical seismic profile, fractures, faults

ABSTRACT

A series of 9 2D and 2D swath surface reflection seismic profiles were acquired over the Brady's Hot Springs producing geothermal field in Churchill County, Nevada. These lines were acquired with much finer source and geophone spacing than that used in typical seismic acquisition. This allowed for more effective filtering of ground roll and other near surface interfering events. Post stack time migration images were produced. Typical of geothermal environments, profiles showed clear coherent reflections over the valley fill, but were less than ideal over the highly faulted producing area. Nonetheless, as discussed by Siler et al., (2016) in a companion paper, the profiles were found to be useful for mapping faults and lithological boundaries.

As part of the same effort, in June 2015, a vertical seismic profile (VSP) survey was conducted at Brady's. The purpose of the survey was to better characterize the subsurface fractures and faults. In conjunction, numerical modeling of fracture impacts on the seismic wave propagation was performed. This modeling suggests that VSP will be more effective than surface reflection seismic for imaging near vertical structures such as faults and fractures. The survey was conducted in a well which is being used for EGS treatment tests at Brady's. A novel high-temperature, 36-level, 3-component, fiber optic accelerometer array with 20 ft spacing between sensor levels was used. The seismic source was a triaxial vibroseis truck capable of generating 3 independent, linear components of ground motion (x, y, and z). Combining the 3 source components with the 3 sensor components at each depth gives a 9-component VSP and allows investigation of the full tensor of seismic wave motion. This type of survey is especially important to aid understanding of converted waves (e.g. P-wave to S-wave) and seismic anisotropy, both of which can be controlled by fracturing and can be used to image fracture/fault zones and potentially invert for fracture properties. Data were recorded between 300 ft and 2020 ft depths, above the EGS reservoir. Initial data analysis and modeling results will be discussed.

1. INTRODUCTION

Fracture stimulation is considered essential for increasing productivity of existing hydrothermal systems as well as engineering new geothermal resources (e.g. Plummer et al., 2015). Successful stimulation requires the presence of pre-existing fractures with favorable orientations (Barton et al., 1995; Ito and Zoback, 2000; Tester, 2006; Davatzes and Hickman, 2009). Accordingly, a critical research and development need for developing geothermal reservoirs is the development of geophysical methodologies which can accurately characterize rock mass fracture and fault systems. These methods must work in the geological environments and at the depths and temperatures commonly encountered in these systems.

Surface seismic reflection and VSP methods have found widespread success in the exploration, development, and production of oil and gas reservoirs, including the characterization of fractured reservoirs (e.g. Far et al., 2013; Maultzsch et al., 2009). In oil and gas environments, sedimentary rocks are often laid down in long nearly horizontal layers. These layers are occasionally cut by faults which lead to vertical offsets of these beds. Seismic reflection profiles over such areas show a series of reflection events which are coherent over long lateral distances. These reflection events often correspond to changes in lithology, and show vertical offsets when cut by faults. As part of the interpretation process, their lateral positions and arrival time on the profile can be identified. With the wealth of velocity data available in these areas, time can be converted to depth, leading to maps of fault locations, bed thickness and depth.

Seismic reflection methods are beginning to see practical use in the geothermal arena (e.g. Melosh et al., 2010; Kell-Hills et al., 2010; Lane et al., 2012; Kent and Louie, 2013; Baujard et al., 2014; Krawczyk et al., 2015; Rabbel et al., 2015; Mellors et al., 2015). In contrast to oil and gas domains, areas with high geothermal potential are commonly in environments dominated by volcanic and metamorphosed rocks, with a high degree of structural complexity. With the exception of valley fill, the long coherent reflection events seen in sedimentary basins are lacking. One further complication in applying reflection seismic methods in geothermal areas is the dearth of velocity information. In many cases, the only available velocity information needed to convert from time to depth are the highly unreliable “normal moveout” (NMO) velocities generated during processing.

Modeling studies (Gritto and Majer, 2003), including some reported here, have suggested that many of these problems can be overcome. They indicate that selection of source and receiver geometries quite different from those used in oil and gas exploration should help overcome some of the structural issues. Finer source and receiver spacings should improve filtering of spatially aliased near surface noise trapped by high to low to high velocity contrasts found in many geothermally altered locations. Use of shear waves has also been proposed for volcanic cover areas. Getting receivers away from the highly attenuating near surface by placing geophones in boreholes

with VSP methods should solve many of the surface noise difficulties. VSP geometries should also be better for detecting the nearly horizontally propagating waves scattered from fractures and faults.

VSP methods are also seeing increased use in geothermal environments (Majer et al., 1988; Daley et al., 1988; Gibson et al., 1995; Thomas and Schulz, 2007; Sausse et al., 2010; Dezayes et al., 2010; Place et al., 2011; Poletto et al., 2013; Lorenzo et al., 2015). VSP is considered one of the most effective tools for providing interval velocity information in support of time to depth conversion of surface reflection seismic data. In addition, Majer et al., 1988 and Daley et al., 1988 reported the use of shear sources and the analysis of fracture related anisotropy. Sausse et al., 2010 showed the direct imaging of fluid conducting faults. However, a major impediment to the widespread application of VSP in geothermal areas is the lack of a modern multi level high temperature VSP sensor string.

With the objective of investigating the effectiveness of these ideas for improving seismic fracture and fault characterization in geothermal areas, a program of surface reflections seismic and VSP data acquisition, processing, and modeling was undertaken. This effort was funded by the Department of Energy, Energy Efficiency and Renewable Energy, Geothermal Technologies Program. Work was focused on the Brady's Hot Springs Known Geothermal Resource Area (KGRA).

2. BRADY'S HOT SPRINGS STUDY AREA

The Brady's Hot Springs geothermal field is located in northwestern Nevada, USA. It has been the subject of geothermal exploration and development since 1959. Geothermal electricity production started in 1992. The Brady's geothermal system supplies fluid to a power station with a total electricity production capacity of 26.4 MWe. It also supplies a direct-use vegetable drying facility.

Heat and permeability at Brady's are controlled by regionally high heat flow (e.g. Lachenbruch and Sass, 1977; Blackwell, 1983) and Basin and Range-style Miocene-recent extensional faulting (Faulds et al., 2010a, b). Brady's, like some ~32% of geothermal systems in the Great Basin, is controlled by a step-over in a normal fault system (Faulds et al., 2006; 2010b; 2011). The step-over at Brady's is a left-step in the west-dipping, north-northeast-striking Brady's fault zone (Figure 1). Geothermal features along the Brady's fault zone include active fumaroles, sinter, calcium carbonate tufa, and silicified sediments (Kratt et al., 2006; Faulds et al., 2012). Equilibrated down-hole fluid temperatures at Brady's have been measured as high as 207°C (Shevenell et al., 2012).

Brady's Hot Springs is also the site of enhanced geothermal stimulation (EGS) testing. This EGS project is partly funded by the Department of Energy, Energy Efficiency and Renewable Energy, Geothermal Technologies Program (Snyder and Zemach, 2013). As part of this research, hydraulic stimulation of the Brady's 15-12 well was planned (Davatzes, et al., 2013). This provided a well of opportunity for conducting VSP measurements.

Figure 1 shows surface faults and geothermal features mapped at Brady's Hot Springs (Faulds et al., 2012; unpublished data). Cultural features such as Interstate 80 cutting diagonally through the study area are also displayed. Surface reflection seismic line common mid point, (also called common depth point (CDP)) locations are exhibited as well. Surface seismic data were acquired in two phases. Phase I lines acquired in 2010 are in green. Phase II lines acquired in 2011 are in red. CDP station numbers are periodically labeled in blue along side each line. VSP source point locations are also presented in red and labeled in blue. Production wells are shown as magenta diamonds. Injector wells are cyan triangles. Observation wells are green circles. The location of the Brady's 15-12 appears as a cyan colored four point star. This is the well planned for hydraulic stimulation as well as VSP acquisition.

The density of faults shown in Figure 1 is quite high, particularly around the cluster of production wells. Mean fault spacing at Brady's Hot Springs is on the order of 250 m (Siler et al., 2016). Fault spacings as low as ~50 m are seen. Using standard seismic industry acquisition spacings for sources and geophones (~30 m), many fault blocks would be covered by only a few image traces. With fault offsets of reflectors occurring every 3 to 4 traces, the seismic images would be very incoherent. Identifying faults from such reflection images is difficult.

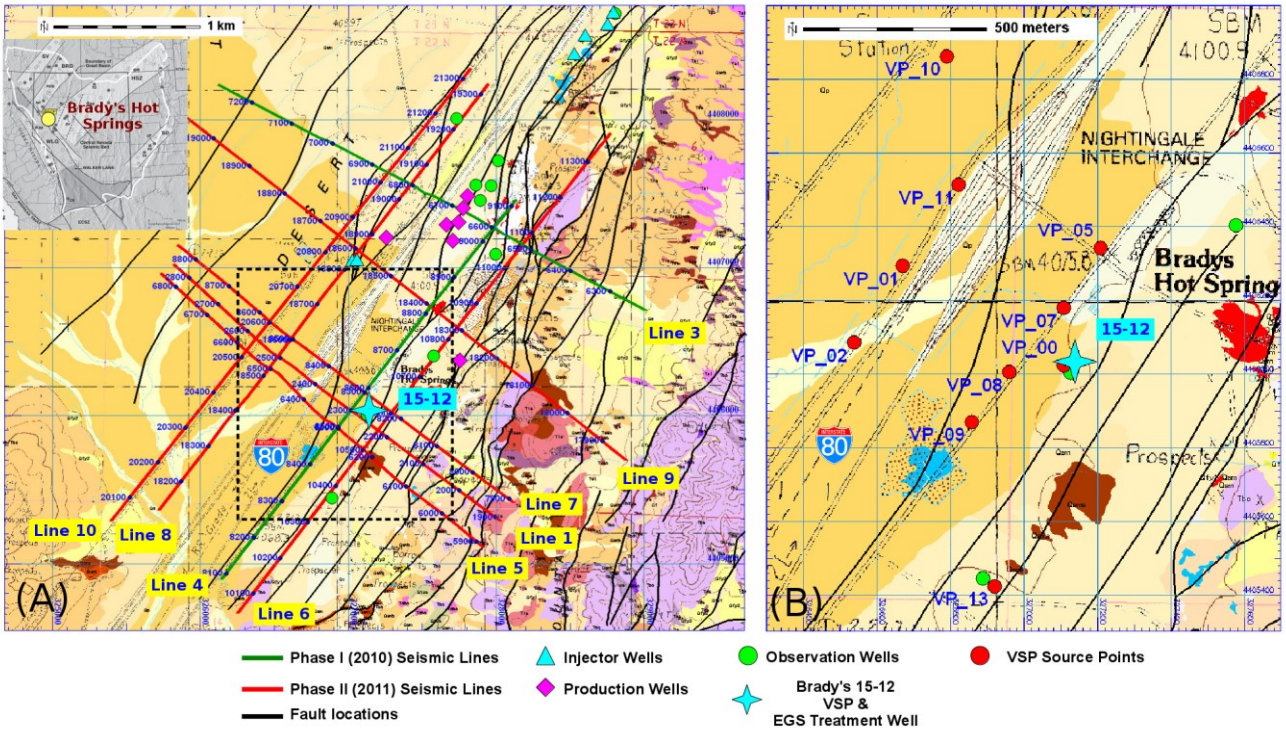

Figure 1: (A) Surface reflection seismic CDP locations and (B) VSP source point locations at Brady's Hot Springs, overlain on a map of surface faults and geothermal features from (Faulds et al., 2012; unpublished data). Dashed rectangle in (A) delineates the area shown in (B). Cultural features such as Interstate 80 cutting diagonally through the study area are also shown.

3. METHODS

3.1 Surface Reflection Seismic Methods

3.1.1 Surface Reflection Seismic Acquisition

A total of 9 surface reflection seismic lines were acquired under Phase I and Phase II of the project over the Brady's Hot Springs KGRA. While 10 lines were originally envisioned, Line 2 was skipped due to access problems. Accordingly, seismic lines are labeled from 1 – 10 with Line 2 absent. Both conventional 2D surface seismic and 2D swath lines were acquired. Lines 1, 3, and 4 were acquired in Phase I. Line 1 was repeated and extended during Phase II, when the remaining 6 lines (4 through 10) were acquired.

Lines 5 through 8 were acquired as 2D swath lines. In swath acquisition, geophones are distributed along one line of ground stations while seismic sources are applied along another parallel offset line of ground stations. For example, seismic images for Line 5 were acquired using geophones along the Line 5 ground stations, with sources applied along Line 1 ground stations. With typical seismic processing, the earth location imaged from a given source and geophone location (CDP) lies at the midpoint between the geophone and source. Accordingly, the image points for swath line 5 lie along a line halfway between the ground station locations for Line 5 and Line 1.

For the acquisition of the surface seismic data, 240 channels were recorded in Phase I. This was increased to 324 channels in Phase II. Geophone and source spacing were nominally 20 ft. (6.1 m), though in some areas a 40 ft. (12.2 m) source spacing was used. This was due to archeological and other cultural constraints such as buildings and highways. A sample rate of 1 ms was used, and record lengths of 4 s were recorded. Sourcing was accomplished using a Bolt Land Air Gun. 8 – 12 pops of the source were stacked at each shot point.

A maximum of 648 vertical geophones were laid out as point receivers. At 20 ft. spacing, this gave approximately 4 km of line length. For conventional 2D recording, shots were recorded from the beginning of the line to the end. With a maximum of 324 live channels, the entire line could not be recorded, so a roll box was used to roll the line. Off end shooting was used, with the source at the lowest active flag of the geophones. This gave a nominal maximum offset of approximately 6400 ft. (1.95 km). Similar strategies were used for the swath lines, with the sources applied on offset lines parallel to the geophone line.

Interstate 80 (I-80) posed a major problem. Aside from the noise generated by traffic, approximately 36 ground stations had to be skipped because of the interstate. In these cases, geophone lines were laid out in two patches of 324 channels each, one on the north-

west side of I-80 and the other on the south-east side. Shots were then acquired from ground stations on both sides of I-80 to each patch, statically (no roll). This allowed undershooting of the section of the line skipped due to the interstate.

3.1.2. Surface Reflection Seismic Processing

Data from both phases of acquisition were processed by the same industry processor (though at two different companies) with experience in the Basin and Range. Basic processing followed the flow: Geometry assignment; elevation Statics; F-X Coherent Noise Suppression in the shot domain; divergence correction (t^1); CDP sort; surface consistent deconvolution; time variant spectral whitening; two passes of velocity and residual statics analysis; application of normal moveout and first break mute; CDP stack; datum correction. A datum velocity of 1400 m/s and datum elevation of 1830 m above mean sea level (AMSL) were used.

After these basic steps, processing broke into two major paths: post stack Kirchoff time migration and pre stack Kirchoff time migration. Within each of these, both random noise attenuation (RNA) and time variant filtering (tvf) were applied.

Pre stack migration results were generally considered to be more robust, and were used in the analysis and interpretation of lines 1, 3, and 4 of the Phase I work. Pre stack migration operates on seismic traces sorted into common offset gathers. Reliable pre stack migration results depend on uniform and extensive coverage. These coverage requirements were met for all lines with the exception of the two swath lines 5 and 7. Due to access restrictions related to permitting, archeology, and roads (including Interstate 80), these two lines suffered severe holes in some of the common offset gathers, and were not considered suitable for pre stack migration. It was felt that these two lines should be included in the overall final interpretation since they bracket the Brady's 15-12 well, the candidate well for future EGS treatment and VSP acquisition. For these reasons, it was decided to use the post stack time migration RNA tvf results for all lines. This insured consistent processing for all the seismic data. Previous comparisons of the pre stack and post stack migration results have shown that there are only minor differences between the two processing results. Figure 1 shows the CDP image point locations for all the post stack time migration seismic data.

All 9 post stack seismic lines were converted to depth using interval velocities derived from NMO stacking velocity analysis. The use of stacking velocities for time to depth conversion is far from ideal. Unfortunately, there were no velocity logs available from the Brady's Hot Springs KGRA. This underscores the need for the development of tools such as high temperature capable VSP which can provide good interval velocity information in geothermal environments.

3.2. Vertical Seismic Profile (VSP) Methods

3.2.1 VSP Acquisition

Vertical seismic profile acquisition utilizes surface sources and borehole sensors. The high temperatures encountered in geothermal wells are a fundamental challenge for acquiring VSP data. They are typically too high for conventional borehole seismic sensors. To address the high temperature issue, a novel fiber optic accelerometer array fabricated by US Sensors Inc. (USSI) was used in the Brady's 15-12 VSP. The sondes in this array were designed to have an operating temperature rating of 200 C, with sensitivity of 1 ng/bit and a frequency range of 3 – 600 Hz. They were clamping wireline deployed units each containing one vertical and two orthogonal horizontal fiber optic accelerometers. The array used in the Brady's 15-12 VSP had 36 sondes spaced at 20 ft. The array was set at three different depths, spanning intervals of 300 – 1000 ft., 1000 – 1700 ft., and 1320 – 2020 ft. relative to the top of the well. Data were acquired by first lowering the array to the shallowest depth, then the intermediate depth, and then the deepest depth. A well bore obstruction was encountered by the bottom sonde at a depth of 2050 ft., preventing acquisition from deeper depths. The well was nearly vertical (deviation less than 0.1 degree) in the depth range covered by the array.

The seismic source was a vibroseis truck, with an unusual triaxial design allowing three components of ground forcing: vertical (P); horizontal-longitudinal (SL); and horizontal-transverse (ST). The horizontal orientations were in-line (SL) and transverse (ST) to the azimuth connecting the source location and the 15-12 well. The vibroseis source used a linear sweep of 8 – 80 Hz, 12 s length with a 0.5 s taper on each end. The specified force output in the vertical mode is about 267 kN and decreases as frequency decreases below 12 Hz. In the horizontal mode, the force output only decreases with decreasing frequency below 5 Hz. The maximum force output in the horizontal mode is about 133 kN, about one-half of the maximum force output in the vertical mode. The combination of three source components and 3 sensor components is known as a 9-component VSP.

Data were acquired using a USSI recording system. Data were recorded at a sample rate of 0.25 ms, with a record length of 15 s. A total of 10 source locations (each with 3 source orientations) were occupied and 4 source sweeps were recorded at each. Source locations were limited by site access, time and funding constraints. Due to time constraints, the decision was made prior to beginning production acquisition to focus imaging to the north-west, west, and south-west of the well. Figure 1A shows the relative locations of the source points and the Brady's 15-12 sensor well.

Production data were recorded for eight hours on June 26, 2015 and two hours on June 27, 2015. Approximately two to three hours were needed to move the array from one depth level to the next. Including rigging up, testing, production acquisition, and rigging down, approximately six days were spent in the field from June 23 – June 28, 2015.

3.2.2 VSP Processing

The VSP data were processed by a second separate oil and gas industry processor. Initial data processing targeted production of a velocity model for compressional and shear waves and generation of upgoing and downgoing wavefields. The processing flow included: Geometry assignment; bandpass filtering of uncorrelated data with filter corner parameters of 3-5-90-100 Hz; vibroseis

correlation with theoretical sweep; bad trace removal and polarity correction of correlated data; stacking for each source location; rotation of horizontal traces into north and east directions; polarity correction of rotated data; F-K filtering for wavefield separation; calculation of velocities.

3.3 Seismic Modeling Methods

In support of acquisition design and interpretation, seismic simulations were run using models of the Brady's Hot Springs KGRA. Two generations of 3D isotropic models of seismic velocities and densities were developed. The first generation of seismic models was based on simple geological models with horizontal lithological beds and a few near vertical faults. After the completion of Phase I reflection data acquisition and processing, the second more sophisticated generation of models were formulated. Depth converted surface seismic reflection profiles from lines 1, 3, and 4 were integrated with well cuttings and core analysis, available well logs, surface mapping of faults and other geological features, and gravity data to produce a geological model. Cross sections from this geological model were then used to build a 3D isotropic geophysical model of the area around the Brady's 15-12 well. Velocities in this model were based on interval velocities inferred from processing generated stacking velocities, augmented by typical values for the given lithologies. Densities were also chosen from typical values. A view of one such 3D model is shown in Figure 2.

In Figure 2, colors represent the compressional wave velocities. The top layer has the datum velocity used in processing the surface reflection seismic data (1830 m/s). Vertical coordinate Z=0 m is at the processing datum elevation of 1400 m above mean sea level (AMSL). The base of the first layer is at ground level. Horizontal X coordinates run from -750 m to 750 m. The Y coordinates start at -250.5 m and end at 250.5 m.

Simulations of surface reflection seismic and VSP were run. The surface location of the simulated Brady's 15-12 VSP well is near the center of the model. The surface location of the simulated well is obscured by the datum layer in the model figure.

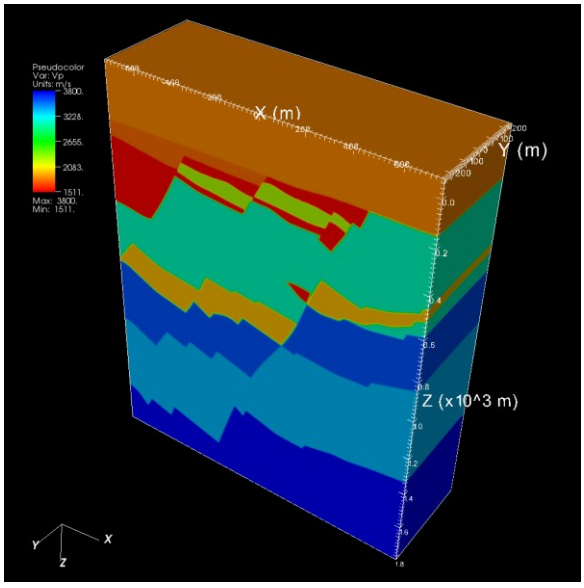

Figure 2: View of the 3D geophysical model from around the vicinity of the Brady's 15-12 well. Colors represent the compressional wave velocities. The horizontal location of the 15-12 well is near the center of the model.

Simulated seismic traces were calculated using an isotropic 3D finite difference staggered grid algorithm (Levander, 1983; Juhlin, 1995). Perfectly matched layer absorbing boundary conditions based on Komatitsch and Martin, (2007) were also implemented.

A grid spacing of 1.5 m and a time step of 0.0001 s were used in the simulations. The seismic wavelet was a Ricker wavelet with a peak frequency of 35 Hz. There were 1001 grid nodes in the X direction, 335 in the Y direction, and 1251 in the Z direction for the model in the figure.

A simpler variation of the model in Figure 2 was also constructed. This model only contained one major fault. Its purpose was to demonstrate the types of events scattered from an individual fault. In all cases, faults were simply modeled by the velocity contrast in offset beds. Features such as fault gouge and damage zones were not included as they were in the modeling of Gritto and Majer (2003).

4. RESULTS

4.1 Modeling Results

4.1.1 Complex Model Results

Figure 3 shows the results of simulations over the complex 3D model. Figures 3(A-D) show 2D XZ plane slices of vertical motion wavefield snapshots at four different times, 0.25 s, 0.40 s, 0.50 s, and 0.75 s respectively. Wavefield amplitudes are shown in gray

scale. The wavefield snapshots are overlain on a color coded 2D slice of the compressional wave velocity grid. Model and snapshots were sliced at the source and geophone Y coordinate of -0.5 m, near the center of the 3D model. The vertical dark purple line shows the location of simulated VSP receivers, and is at the location of the Brady's 15-12 well relative to the geological model. The two magenta horizontal lines at depths of approximately 257 m and 775 m below datum bracket the depth intervals covered by the actual VSP measurements. The yellow circle represents the simulated vertical force source location with horizontal offset of 46.5 m from the well. The cyan colored horizontal line gives the location of the simulated 2D surface reflection seismic array.

The events circled in yellow on the wavefield snapshots are near surface waves trapped in the low to high to low near surface velocity layers. They move horizontally across the model with time, until they reach offset beds of a near surface fault. There they begin to scatter, with scattered energy moving back in the opposite direction. Figure 3E shows the simulated vertical geophone surface seismic common source gather plotted with trace spacings and offsets typical of the actual field acquisition of the surface seismic data. The back scattered near surface waves are circled in yellow. They are a dominant feature of the simulated common source gather.

The wavefield circled in magenta in Figure 3A shows the down going direct compressional wave impinging on the offset beds of the major fault in the model (vertical fault offset of approximately 250 m). The wavefield circled in magenta in Figure 3B at time of 0.40 s shows the compressional wave scattered from this fault as it crosses the VSP array at depths of approximately 650 m to 730 m. It is barely discernible and suffers from strong interference from down going multiples and other scattered events. Figure 3F shows the simulated vertical VSP traces plotted with the same depths and spacings as the actual field data. The events circled in magenta are at the same time and depths as the magenta area circled in Figure 3B.

The wavefield circled in green in Figure 3C is the direct down going shear wave as it encounters the offset beds of the major fault. The area circled in green in Figure 3D shows the scattered wavefield generated by this encounter as it crosses the VSP array. In contrast to the wavefield circled in Figure 3B, this wavefield is quite strong and is relatively free of interference. The event underlined in green in the simulated VSP (Figure 3F) is at the same time and depths as the green circled area in Figure 3D.

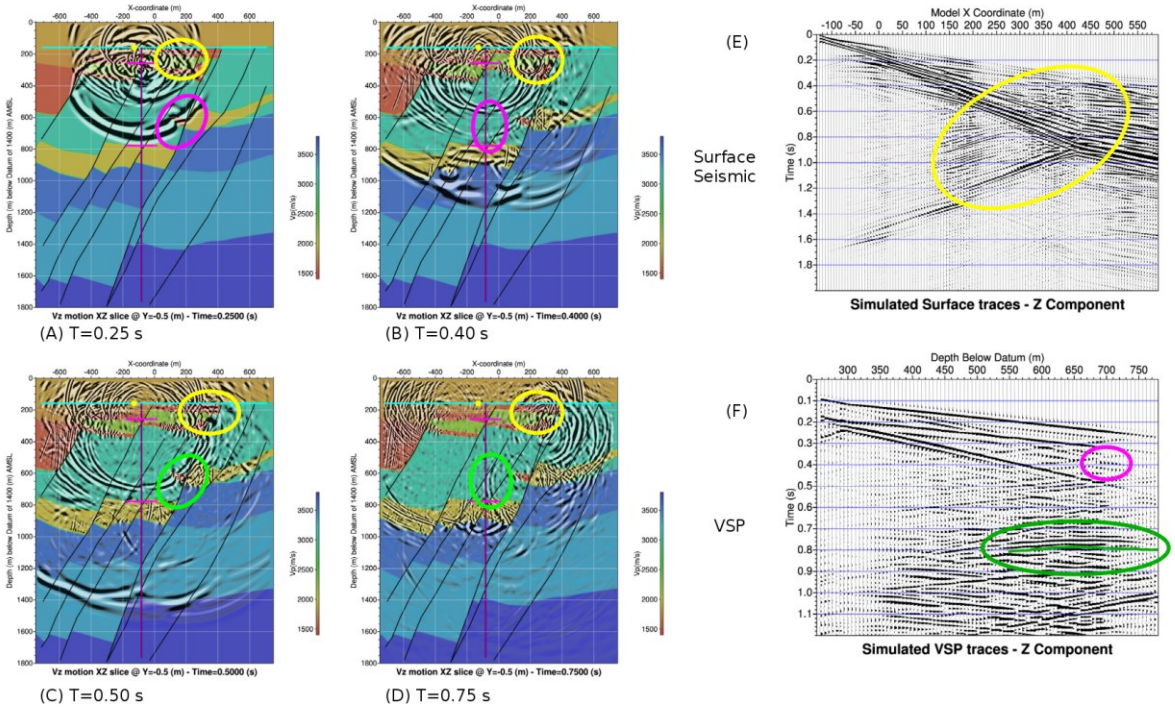

Figure 3: Complex model simulation results.

4.1.2 Simplified Model Results

Figure 4 shows similar results from the simplified model. This model only contains one fault, and has horizontal beds. Arrival times of the various waves differ from Figure 3 because of the slightly different velocity structure. Again, the back scattered near surface trapped waves circled in yellow are seen to dominate the surface reflection common shot gather. The scattered wavefield from the down going compressional wave is slightly more visible in Figure 4B. It still suffers from interference from multiples as well as the down going direct shear wave. The wavefield scattered by the fault from the down going shear wave (Figure 4D, circled in green) is seen to be clear, though somewhat different in character from that shown in Figure 3D. There is also a strong corresponding event underlined in green in the simulated VSP of Figure 4F.

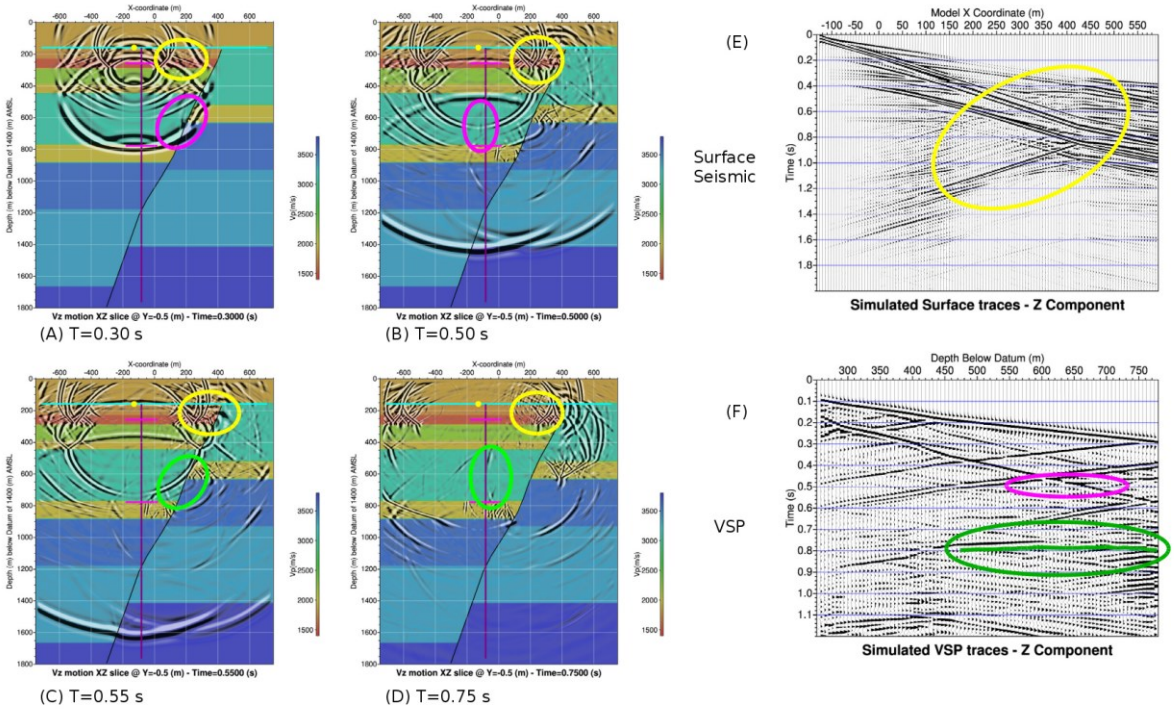

Figure 4: Simple model simulation results.

4.2 VSP Results

Figure 5 shows time vs. depth VSP traces acquired from the vertical vibrator at the near offset (= ~32 m) source point (VP_00 in Figure 1B). This offset is similar to the offset of the source in the model simulations. Figure 5 (A) and (B) are the east and north oriented traces after rotation. Traces have been divergence corrected, and each trace has been normalized with the maximum amplitude set to one. The event highlighted in green on the vertical traces (Figure 5C) is at approximately the same time and depths as the event shown in green in the modeling results (Figures 3F and 4F). This event has an apparent velocity (inverse of the slope of the event) much higher than the apparent velocities of the up and down going compressional and shear waves. It is not apparent on the horizontal east or north oriented traces.

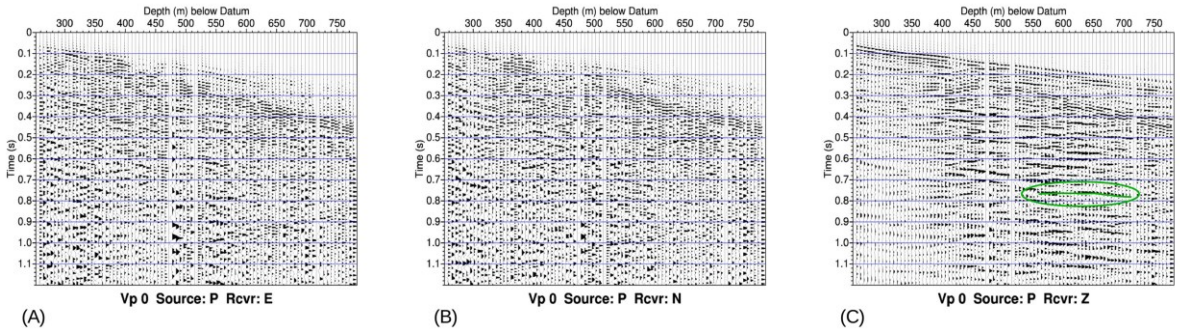

Figure 5: VSP traces from a vertical vibrator at the near offset source point Vp 0. (A) and (B) are the horizontal east and north oriented traces after rotation respectively. The event highlighted in green on (C) (vertical traces) is at approximately the same time and depths as the event shown in green in the modeling results.

Figure 6 shows similar plots for the traces from the vertical vibrator at source point 8 (offset = ~ 181 m, VP_08 in figure 1B). This source point is almost due west of the well. East oriented horizontal traces (Figure 6A) approximately correspond to the SL direction and north oriented horizontal traces (Figure 6B) to the ST direction.

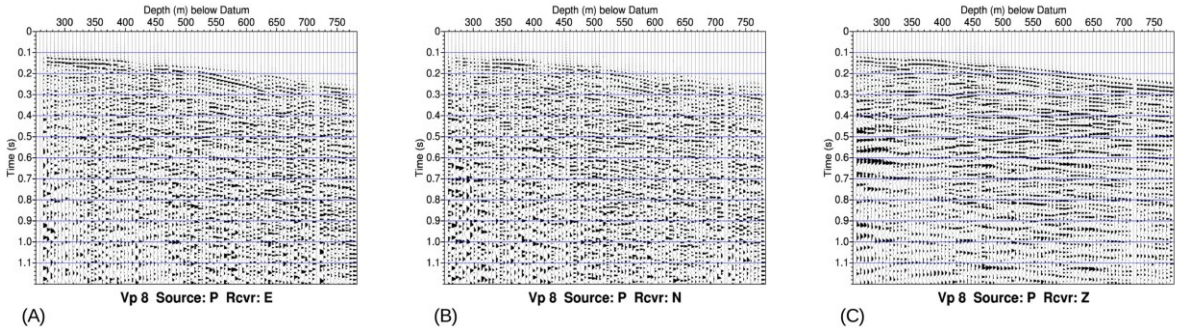

Figure 6: VSP traces from a vertical vibrator at source point Vp 8. (A) and (B) are the horizontal east and north oriented traces after rotation respectively. The source point is almost due west of the receiver array. (C) are vertical traces.

Figure 7 shows the compressional and shear interval velocities inverted from first break picks of the near offset VSP (Figure 5).

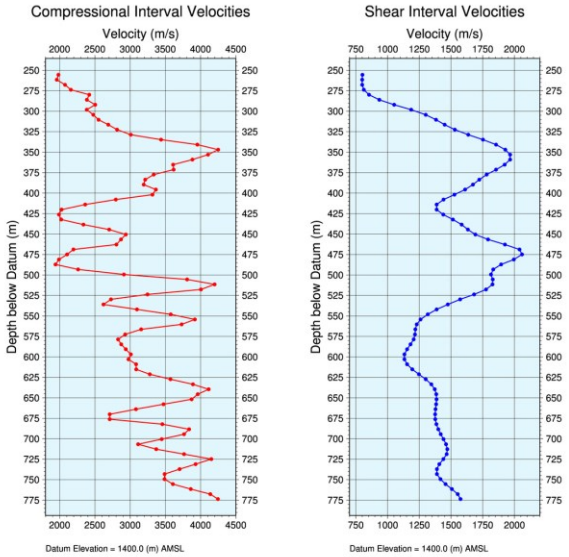

Figure 7: Inverted compressional and shear interval velocities from the near offset source point VSP (Figure 5).

4.3 Surface Reflection Seismic Results

Figure 8 shows the time to depth converted post stack migration reflection seismic results for Line 3. As seen from Figure 1, this line runs south-east to north-west through the main production area at Brady's Hot Springs. The color trace display is overlain by colors representing the compressional interval velocities inverted from the processing NMO velocities. Downhole lithological data are also displayed for nearby wells. Lithological characterizations were derived from analysis of cuttings and core from a total of 21 wells, as described by Siler et al., (2016), and correlating such analyses with detailed mapping in the area (Faulds et al., 2012). Nearby well data were projected horizontally onto the line along an azimuth of 30° from north, the nominal strike direction of Brady's structures. A simple Bouger anomaly profile (Muir, 2012) extracted along the line is posted at the top of the section. Intersecting line locations are shown in white.

As described by Siler et al., (2016), geological mapping, core and cuttings lithological analysis, four geological cross sections, and the interpretation of the nine seismic lines discussed here were integrated into an overall 3D geological model of the Brady's Hot Springs KGRA. Horizon and fault picks from that model that intersected the line are also shown.

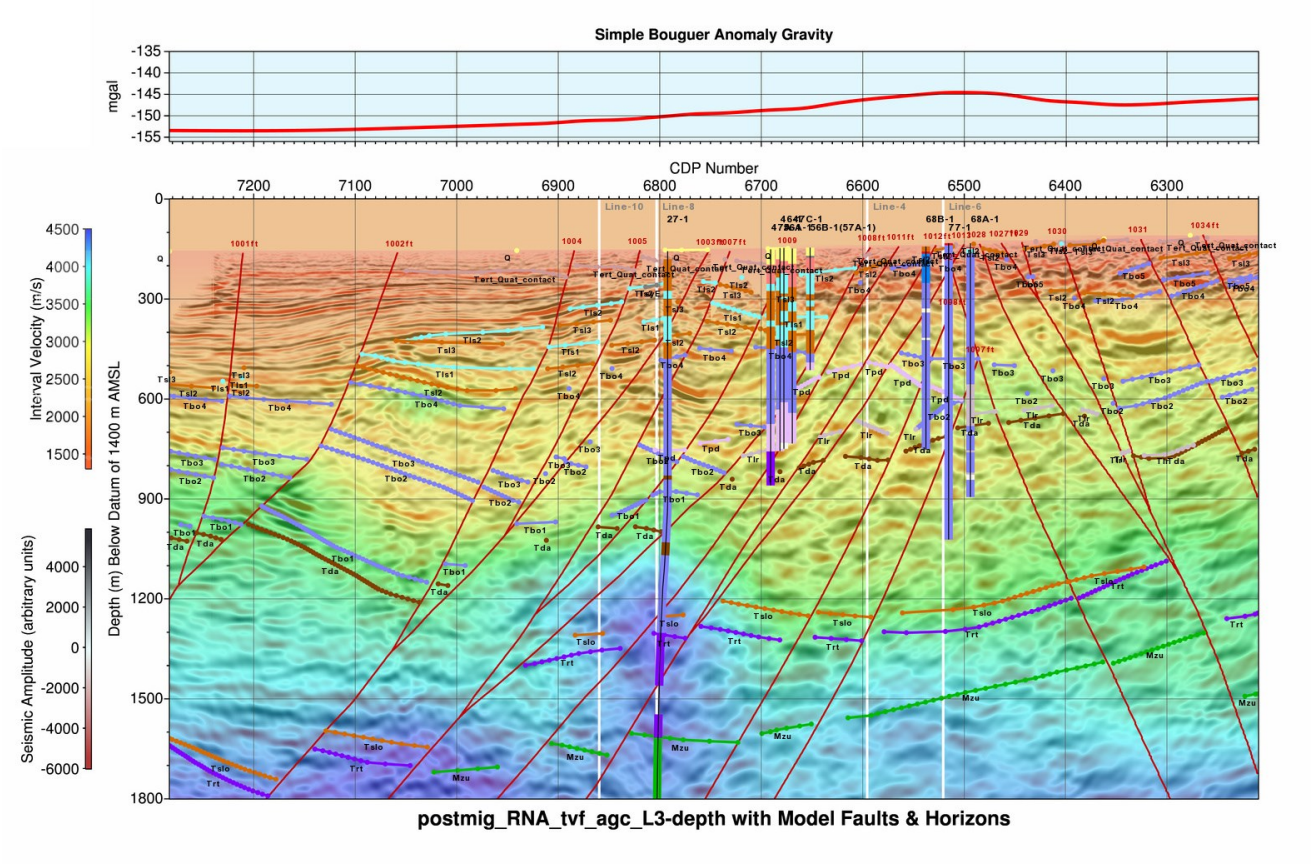

Figure 8: Line 3 post migration color coded seismic traces overlain by color coded interval velocities, well lithologies, and 3D geological model horizon and fault picks. A simple Bouger anomaly profile extracted along the line is shown at the top. Intersecting line locations are shown in white. This line passes through the main production area.

Lithology Codes

COLOR	CODE	DESCRIPTION
	Mzm, Mzu	Mesozoic undistinguished
	Qf	Alluvial fan deposits
	Tu	Tertiary undistinguished
	Tabo	Older basaltic lavas, altered
	Tbo	Older basaltic lavas
	Tda	Andesite-dacite lavas
	Tls	Limestone
	Trt	Oligocene ash-flow tuffs
	Tlr	Rhyolite lavas and lesser tuffs
	Tsl	Lacustrine sediments
	Tslo	Older lacustrine sediments
	Tslo+Tlr	Tslo+Tlr
	Tsy	Sandstone and conglomerate
	Tts	Non-welded tuffs
	Tpd	Porphyritic Hb-Bt dacite to rhyodacite flows and domes

Figure 9: Lithology color codes for the horizons and well lithologies shown in Figures 8 and 10.

Figure 10 shows a plot similar to Figure 8, but for Line 1. Line 1 also runs from south-east to north-west (see Figure 1). The Brady's 15-12 well is the third well from the left. This is the well used in the VSP acquisition. It is also the well selected for EGS treatment. Five fault traces from the 3D geological model are seen to intersect the 15-12 well. Surface locations of these faults are known from surface mapping. Their depths in the well are known from where they cut through core taken from the nearby (~30 m) BCH-3 well.

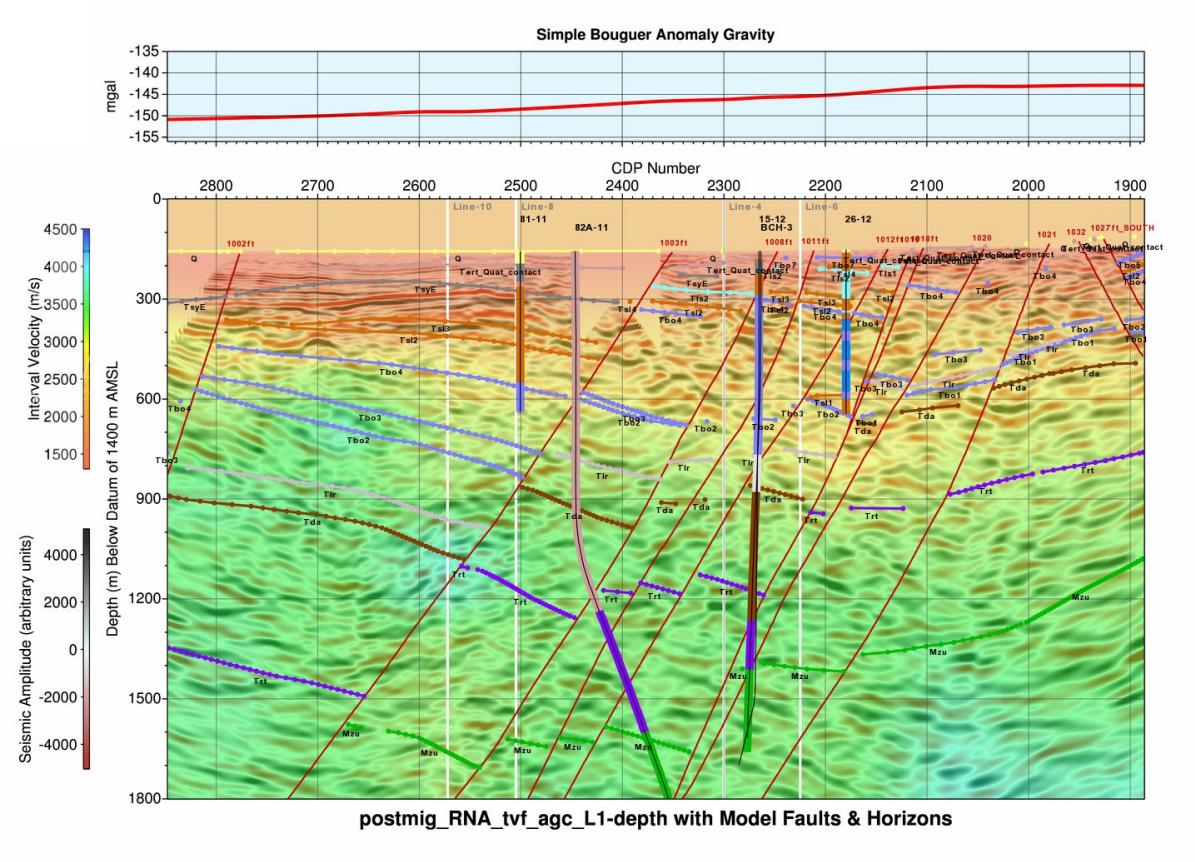

Figure 10: Line 1 post migration color coded seismic traces overlain by color coded interval velocities, well lithologies, and 3D geological model horizon and fault picks. A simple Bouger anomaly profile extracted along the line is shown at the top. Intersecting line locations are shown in white. This line passes near the Brady's 15-12 well (third well from the left), the well used in the VSP acquisition and planned EGS treatment.

Similar plots were created for the remaining seven seismic lines. These plots were then interpreted and integrated into the overall building of the 3D geological model.

Figure 11 shows a common shot gather from Line 1. The source is located at CDP 2302. The apparent backscattered energy originates near offset 600 m, which corresponds to CDP 2104. This is the CDP location where a major fault is seen to break the surface in Figure 10. These events would be aliased at normal seismic spacing. The events from 0 to ~150 m offset are spatially aliased even at the fine spacing used in the acquisition. Fortunately, these events could be muted without losing much of the deeper reflection information.

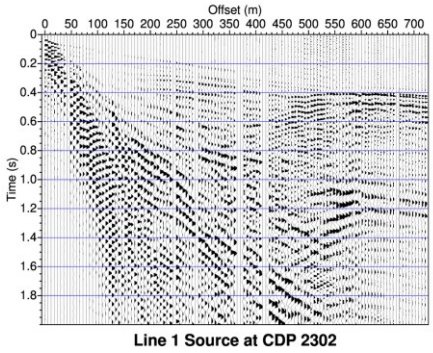

11: Common source gather from Line 1. Source is at CDP 2302. Trace at offset 601 m is at CDP 2104

5. DISCUSSION

The modeling demonstrates some of the impact of faulting on both the surface reflection seismic and the VSP data. Surface seismic is dominated by fault scattered events from the near surface. Energy scattered from deeper segments of faults is seen to propagate almost horizontally. Such events never really reach the surface seismic array. These horizontally moving events do strike the VSP array at depth. They generate visible events with extremely fast apparent velocities on the VSP synthetic traces.

One limitation of the modeling presented here is the lack of attenuation. Shear events in particular show much higher amplitudes in the synthetic traces than are actually observed in field data (compare Figures 3F and 5C). There is also a need to include properties controlling fault and fracture compliance (e.g. thickness, filling material, contact area) in order to generate scattering when no offset beds are present. Such scattering is also expected to generate horizontally propagating events with very high apparent-velocity in VSP (Gritto and Majer, 2003), similar to the offset bed scattering. Amplitudes, polarizations, and frequencies of these scattered events should carry information about the internal geometry and filling material of the faults and fractures.

The VSP data show a number of events with very high apparent-velocity (Figures 5 and 6), some at the same depths and time predicted by the modeling (Figure 5C). Modeling suggests that these events in the VSP data are fault scattered events. Unfortunately, many things besides fault scattering can cause such events, including interfering up and down going bed reflections. To truly qualify these events as scattering from faults or fractures processing beyond the scope of this project would be needed. Reverse time migration such as discussed by Wang et al., (2011) would be beneficial, but the available source points may not be optimal for such imaging.

The VSP did produce important velocity information down to depths of 775 m below datum (Figure 7). Comparison of the arrival times of the down going compressional waves (first breaks) in Figures 5C, 3F and 4F shows that the velocities in the model are slightly slow. Incorporation of these new VSP interval velocity estimates would improve both the modeling and the time to depth conversion of the surface reflection data in the vicinity of the VSP well (Figure 10).

The geological model overlain on the reflection seismic results in Figures 8 and 10 shows a very complex structure for the Brady's Hot Springs KGRA. In spite of this complexity, tracking the Trt horizon (purple horizon on Figures 8 and 10) shows that only two major faults offset the beds along these two seismic lines.

Along Line 3 (Figure 8) which passes through the producing area, the first major fault (from the left) intersects the surface near CDP 6590. It is labeled as fault 1003ft in the figure. This fault dips to the north-west and has a vertical offset of approximately 300 m. The second major fault along Line 3 cuts the surface near CDP 6405 (fault 1030) and dips to the south-east with approximately 200 m of vertical offset.

Line 1 (Figure 10) passes near the Brady's 15-12 VSP/EGS well. It crosses a major fault breaking the surface near CDP 2350 (fault 1003ft), the same fault as the first major fault along Line 3. It dips to the north-west and has an offset of near 250 m at this location. The top of the second major fault along Line 1 is near CDP 2105, labeled as fault 1018ft. This fault also dips to the north-west with offset of around 250 m. It is the fault included in the simplified 3D model of Figure 4 and cuts through the Brady's 15-12 well.

A number of short but continuous reflections are visible along these lines near these faults. Examples along Line 3 are: between CDP's 6900 and 6600 at depth of ~550 m; between CDP's 7280 and 6980 at depth of ~1500 m; and between CDP's 6370 and 6300 at depth of ~450 m. A Line 1 example is between CDP's 2290 and 2150 at depths between ~440 m and ~520 m. This Line 1 reflection event is also visible in the near offset VSP results (Figure 5). Figure 5 shows a reflected up going event originating at a depth of ~480 m.

In each of these cases, the reflection is seen to terminate against a major fault in the surface reflection seismic data. These terminations were considered useful (though not definitive) when combined with other geological data in constraining the subsurface locations of faults. No events interpreted as fault plane reflections have been identified. The standard seismic processing applied to these data tends to remove any horizontally moving events, such as those scattered from faults, which survive to reach the surface

Usual oil and gas industry reflection seismic geophone and shot spacings range from 55 ft to 220 ft. In this work, spacings up to 10 times finer were used. These finer spacings were effective in reducing the spatial aliasing of near surface source related noise (e.g. “ground roll”). They also allowed for the use of very long noise attenuation filters during processing. Over zones with small fault spacings, they provided better resolution of diffraction arcs generated by short reflection segments between faults.

The backscattered energy seen in Line 1 shot gather traces (Figure 11) originates at the offset where fault 1018ft breaks the surface. The modeling suggests that this backscattered energy is caused by near surface waves scattering off the fault, which carry no information about the structure of the deeper fault. These backscattered events cut across the reflections from deeper beds, and cannot be simply muted out. They could only be filtered out of the data (revealing reflections below) because they are not spatially aliased. At standard seismic acquisition spacings, these events would have been spatially aliased, leading to a much poorer reflection image. Only the use of fine spacing has allowed the removal of these events. Melosh et al., (2010) have reported on the contamination of surface reflection seismic profiles by near surface waves which resulted in apparent events erroneously interpreted as fault plane reflections.

6. CONCLUSIONS

The use of surface seismic reflection data at Brady's Hot Springs was found useful in building a geological model, but only when combined with other extensive geological and geophysical data. The use of fine source and geophone spacing was critical in producing useful images. The surface seismic reflection data gave no information about the internal structure (extent, thickness and filling) of faults and fractures, and modeling suggests that they are unlikely to do so.

Modeling does indicate that VSP and other seismic methods with sensors located at depth in wells will be the most effective seismic tools for getting information on the internal structure of faults and fractures in support of fluid flow pathway management and EGS treatment. Scattered events similar to those expected from faults and fractures are seen in the VSP reported here. Unfortunately, the source offset and well depth coverage do not allow for detailed analysis of these events. More extensive acquisition is needed to support fault and fracture characterization in the geothermal reservoir at Brady's Hot Springs.

The VSP was effective in generating interval velocity estimates over the depths covered by the array. Upgoing reflection events are also visible in the VSP results at locations corresponding to reflection events in the surface seismic. Overall, the high temperature rated fiber optic sensors used in the VSP produced useful results.

Modeling has been found useful in the interpretation of both surface reflection seismic and VSP data. It has helped identify possible near surface scattering in the surface seismic data. It has highlighted potential scattering events from deeper faults in the VSP data. Inclusion of more detailed fault and fracture specific stiffness parameters are needed to fully interpret fault and fracture scattered events for internal structure and filling.

7. ACKNOWLEDGMENTS

This material is based upon work supported by the Department of Energy, Energy Efficiency and Renewable Energy, Geothermal Technologies Program under Award Number DE-FG36-08GO18191. We thank Ormat Technologies, Inc. for their contributions as a major participant in this project giving extensive access to their data and to the Brady's Hot Springs KGRA. We thank the organization of Stephen G. Muir, Consulting Geologist and Geophysicist, and Steve in particular, for their contributions as a major participant in this project. They have been the seismic contractor acquiring all of the surface seismic data, and have contributed a significant amount of their field time in acquiring the seismic and gravity data. We thank Michelle Robertson of LBNL for acquisition supervision and support, USSI for sensor design, and data acquisition support and Cecil Hoffpauir of UT Austin for vibroseis source support. Paulsson Inc. performed initial VSP data processing. Work at Lawrence Berkeley National Laboratory was supported by the Geothermal Technologies Program under Contract No. DE-AC02-05CH11231.

REFERENCES

Barton, C.A., Zoback, M.D., and Moos, D., 1995, Fluid flow along potentially active faults in crystalline rock: *Geology*, **23**, no. 8, 23–27, doi: 10.1130/0091-7613(1995)023<0683:FFAPAF>2.3.CO;2.

Baujard, C., Genter, A., Maurer, V., Dalmais, E., Graff, J., and Schmittbuhl, J., 2014, The ECOGI EGS Project in Rittershoffen, France, *Geothermal Resources Council Transactions*, **38**, 267–270.

Blackwell, D.D., 1983, Heat flow in the northern Basin and Range province: *Geothermal Resources Council, Special Repor*t **13**, 81–93.

Daley, T.M., McEvilly, T.V., and Majer, E.L., 1988, Analysis of P and S wave Vertical Seismic Profile Data From the Salton Sea Scientific Drilling Project, *Journal of Geophysical Research: Solid Earth*, **93**(B11), 13025-13036, doi 10.1029/JB093iB11p13025.

Davatzes, N.C., and Hickman, S., 2009, Stress and Fluid Flow Prior to Stimulation of Well 27-15, Desert Peak, Nevada, EGS Project, *Proceedings*, 34th Workshop on Geothermal Reservoir Engineering, Stanford University, Stanford, CA.

Davatzes, N.C., Feigl, K., Mellors, R.J., Foxall, W., Wang, H.F., and Drakos, P., 2013, PRELIMINARY INVESTIGATION OF RESERVOIR DYNAMICS MONITORED THROUGH COMBINED SURFACE DEFORMATION AND MICRO-EARTHQUAKE ACTIVITY: BRADY'S GEOTHERMAL FIELD, NEVADA, *Proceedings*, 38th Workshop on Geothermal Reservoir Engineering, Stanford University, Stanford, CA.

Dezayes, C., Genter, A., and Valley, B., 2010, Overview of the Fracture Network at Different Scales Within the Granite Reservoir of the EGS Soultz Site (Alsace, France), *Proceedings*, World Geothermal Congress 2010, Bali, Indonesia, 25-29 April, 2010.

Far, M.E., Sayers, C.M., Thomsen, L., Han, D., and Castagna, J.P., 2013, Seismic characterization of naturally fractured reservoirs using amplitude versus offset and azimuth analysis, *Geophysical Prospecting*, **61**, 427-447, doi: 10.1111/1365-2478.12011.

Faulds, J.E., Coolbaugh, M.F., Vice, G.S., and Edwards, M.L., 2006, Characterizing Structural Controls of Geothermal Fields in the Northwestern Great Basin: A Progress Report: *Geothermal Resources Council Transactions*, **30**, 69–76.

Faulds, J.E., Coolbaugh, M.F., Benoit, W.R., Oppliger, G.L., Perkins, M., Moeck, I., and Drakos, P.S., 2010a, Structural Controls of Geothermal Activity in the Northern Hot Springs Mountains, Western Nevada: The Tale of Three Geothermal Systems (Brady's, Desert Peak, and Desert Queen): *Geothermal Resources Council Transactions*, **34**, 675–684.

Faulds, J.E., Moeck, I., Drakos, P.S., and Zemach, E., 2010b, Structural Assessment and 3D geologic modeling of the Brady's geothermal area, Churchill County (Nevada, USA): A preliminary report, *Proceedings*, 35th Workshop on Geothermal Reservoir Engineering, Stanford University, Stanford, CA, 298–302.

Faulds, J.E., Hinz, N.H., Coolbaugh, M.F., Cashman, P.H., Kratt, C., Dering, G.M., Edwards, J., Mayhew, B., and Mclachlan, H., 2011, Assessment of Favorable Structural Settings of Geothermal Systems in the Great Basin, Western USA: *Geothermal Resources Council Transactions*, **35**, 777–784.

Faulds, J.E., Ramelli, A.R., Garside, L.J., Coolbaugh, M.F., and Green, H.L., 2012, Preliminary geologic map of the Desert Peak Quadrangle, Churchill County, Nevada: *Nevada Bureau of Mines and Geology Open-File Report* **12-5**, scale 1:24,000:.

Gibson, R.L., Lee, J.M., Toksöz, M.N., Dini, I., and Cameli, G.M, 1995, Three-dimensional Kirchoff Migration Analysis of VSP Data From a Geothermal Field, *Proceeding*s, World Geothermal Congress, 1995, International Geothermal Association, 2, 869-873.

Gritto, R., and Majer, E.L., 2003, Seismic Methods for Resource Exploration in Enhanced Geothermal Systems, *Geothermal Resources Council Transactions*, **27**, 223–226.

Ito, T., and Zoback, M.D., 2000, Fracture permeability and in situ stress to 7 km depth in the KTB Scientific Drillhole, *Geophysical Research Letters*, **27**, no. 7, 1045-1048, doi: 10.1029/1999GL011068.

Juhlin, C., 1995, Finite-difference elastic wave propagation in 2D heterogeneous transversely isotropic media, *Geophysical Prospecting*, **43**, no. 6, 833-858, doi: 10.1111/j.1365-2478.1995.tb00284.x.

Kell-Hills, A., Louie, J., Kent, G., Pullammanappallil, S., Sabin, A., and Lazarro, M., 2010, A Revised Interpretation of 3D Seismic Data, Hawthorne Army Depot, Nevada: Faulted-Basin Reflections or Sill Intrusions?, *Geothermal Resources Council Transactions*, **34**, 869–872.

Kent., T., and Louie, J.N., 2013, TECTONIC DEFORMATION OF A LACUSTRINE MUDSTONE AT SODA LAKE GEOTHERMAL FIELD, WESTERN NEVADA, USA, FROM 3D SEISMIC INTERPRETATION, *Proceedings*, 35th New Zealand Geothermal Workshop, 17-20 November 2013, Rotorua, New Zealand.

Komatitsch, D., and Martin, R., 2007, An unsplit convolutional perfectly matched layer improved at grazing incidence for the seismic wave equation, *Geophysics*, **72**, no. 5, SM155-SM167, doi: 10.1190/1.2757586.

Kratt, C., Calvin, W., and Coolbaugh, M.F., 2006, Geothermal exploration with Hymap hyperspectral data at Brady–Desert Peak, Nevada: *Remote Sensing of Environment*, **104**, no. 3, 313–324, doi: 10.1016/j.rse.2006.05.005.

Krawczyk, C., Polom, U., Wiyono, and Pramono, B., 2015, Tailoring Reflection Seismic Experiments to Geothermal Exploration Targets in Indonesia – Wayang Windu Geothermal Field Case Study, *Proceedings*, World Geothermal Congress, Melbourne, Australia, 19-25 April, 2015.

Lachenbruch, A.H., and Sass, J.H., 1977, Heat flow in the United States and the thermal regime of the crust, in Heacock, J.G. ed., The Nature and Physical Properties of the Earth's Crust, *American Geophysical Union Monograph*, 626–675.

Lane, M., Schweickert, R., and DeRocher, T., 2012, USE OF SEISMIC IMAGING TO IDENTIFY GEOTHERMAL RESERVOIRS AT THE HOT POT AREA, NEVADA, *Proceedings*, 37th Workshop on Geothermal Reservoir Engineering, Stanford University, Stanford, CA.

Levander, A.R., 1998, Fourth-order finite-difference P-SV seismograms, *Geophysics*, **53**, no. 11, 1425-1436, doi: 10.1190/1.1442422.

Lorenzo, C., Soto, J, Palma, H., Diez, H., and Pérez, H., 2015, Vertical Seismic Profile (VSP) in the Injection Well AZ-03, Los Azufres Geothermal Field, México, *Proceedings*, World Geothermal Congress, Melbourne, Australia, 19-25 April, 2015.

Majer, E.L., McEvilly, T.V., Eastwood, F.S., and Myer, L.R., 1988, Fracture detection using P-wave and S-wave vertical seismic profiling at The Geysers, *Geophysics*, **53**, no. 1, 76-84, doi: 10.1190/1.1442401.

Maultzsch, S., Nawab, R., Yuh, S., Idrees, M., and Frignet, B., 2009, An integrated multi-azimuth VSP study for fracture characterization in the vicinity of a well, *Geophysical Prospecting*, **57**, 263-274, doi: 10.1111/j.1365-2478.2008.00769.x.

Mellors, R.J., Marks N., Pullammnappellil, S., Casteel, J., Yang, T., Moore, J., and Jones, C.G., 2015, Imaging Geothermal Resources with 3D Seismic Attributes, *Proceedings*, 40th Workshop on Geothermal Reservoir Engineering, Stanford University, Stanford, CA.

Melosh, G., Cumming, W., Casteel, J., Niggemann, K., and Fairbank, B., 2010, Seismic Reflection Data and Conceptual Models for Geothermal Development in Nevada, *Proceedings*, World Geothermal Congress, Bali, Indonesia, 25-29 April, 2010.

Muir, S.G., 2012, personal communication.

Place, J., Le Garzic, E., Geraud, Y., Diraison, M., and Sausse, J., 2011, CHARACTERISATION OF THE STRUCTURAL CONTROL ON FLUID FLOW PATHS IN FRACTURED GRANITES, *Proceedings*, 36th Workshop on Geothermal Reservoir Engineering, Stanford University, Stanford, CA.

Plummer, M., Huang, H., Podgorney, R., Moore, J., and Bradford, J., 2015, Reservoir Response to Thermal and High-pressure Well Stimulation Efforts at Raft River, Idaho, *Proceedings*, 40th Workshop on Geothermal Reservoir Engineering, Stanford University, Stanford, CA.

Poletto, F., Corubolo, P., Biancamaria, F., Schleifer, A., Petronio, L., and Vedova, B.D., 2013, Multi-offset VSP for the integrated geophysical characterization of the Grado (NE Italy) carbonatic reservoir, *Proceedings*, European Geothermal Congress 2013, Pisa, Italy, 3-7 June, 2013.

Rabbel, W., Thorwart, M., Behrendt, N., Holzrichter, N., Niederau, J., Ebigbo, a., Marquart, G., Dini, I., and Ciuffi, S., 2015, A Stochastic Assessment of Geothermal Potential Based on Seismic and Potential Field Analysis and Hydro-thermal Forward Modeling – an Example from Tuscany (Italy), *Proceedings*, World Geothermal Congress, Melbourne, Australia, 19-25 April, 2015.

Sausse, J., Dezayes, C., Dorbath, L., Genter, A., and Place, J., 2010, 3D model of fracture zones at Soultz-sous-Forêts based on geological data, image logs, induced microseismicity and vertical seismic profiles, *Comptes Rendus Geoscience*, **342**, 531-545, doi: 10.1016/j.crte.2010.01.011.

Shevenell, L.A., Oppliger, G., Coolbaugh, M.F., and Faulds, J.E., 2012, Bradys (Nevada) InSAR Anomaly Evaluated With Historical Well Temperature and Pressure Data: *Geothermal Resources Council Transactions*, **36**, 1383–1390.

Siler, D.L., Faulds, J.E., Hinz, N.H., and Queen, J.H., 2016, 3D analysis of geothermal fluid flow favorability; Brady's, Nevada, USA, *Proceedings*, 41st Workshop on Geothermal Reservoir Engineering, Stanford University, Stanford, CA (submitted).

Snyder, K., and Zemach, E., 2013, Bradys EGS Project, Presentations, Department of Energy, Energy Efficiency and Renewable Energy, Geothermal Technologies Program 2013 *Peer Review*, Denver, CO, April 22-25, 2013, (http://energy.gov/eere/geothermal/downloads/bradys-egs-project-0)

Tester, J., editor, 2006, The future of geothermal energy: impact of Enhanced Geothermal Systems (EGS) on the United States in the 21st century. Massachusetts Institute of Technology.

Thomas, R., and Schulz, R., 2007, Facies Differentiation of the Malm by Interpretation of Reflection Seismic Profiles and a Moving Source VSP Experiment, *Proceedings*, European Geothermal Congress 2007, Unterhaching, Germany, 30 May – 1 June 2007.

Wang, Y., Huang, L., and Zhang, Z., 2011, Reverse-time Migration of Time-lapse Walkaway VSP Data For Monitoring CO2 Injection At the SACROC EOR Field, *SEG Technical Program Expanded Abstracts 2011*, 4304-4308, doi: 10.1190/1.3628107.